Supplement of Geosci. Model Dev., 19, 10283–10308, 2026
https://doi.org/10.5194/gmd-19-10283-2026-supplement
© Author(s) 2026. CC BY 4.0 License.



Geoscientific Model Development
Open Access
EGU

Supplement of

EnsAI: an emulator for atmospheric ammonia ensembles

Michael Sitwell

Correspondence to: Michael Sitwell (michael.sitwell@ec.gc.ca)

The copyright of individual parts of the supplement might differ from the article licence.

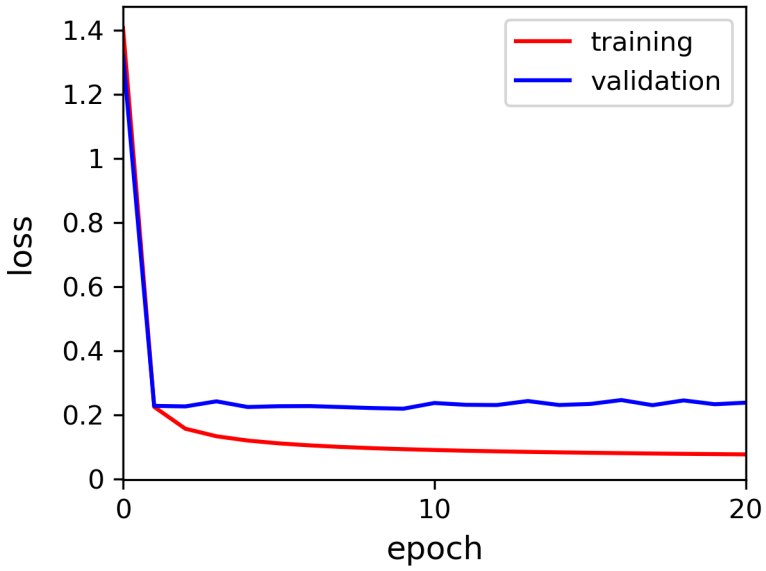


Figure S1. The learning curve produced during the training of the EnsAI model.

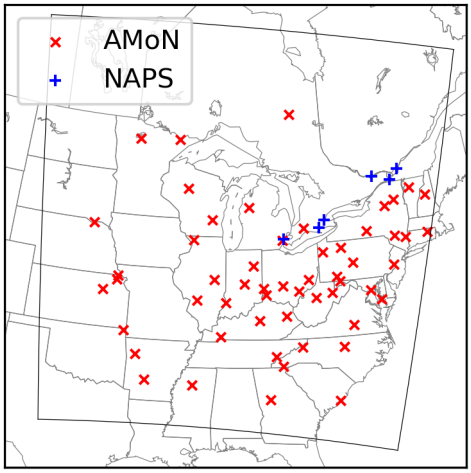


Figure S2. AMoN and NAPS station locations within the EnsAI model domain that have valid observations for the test period (2015).

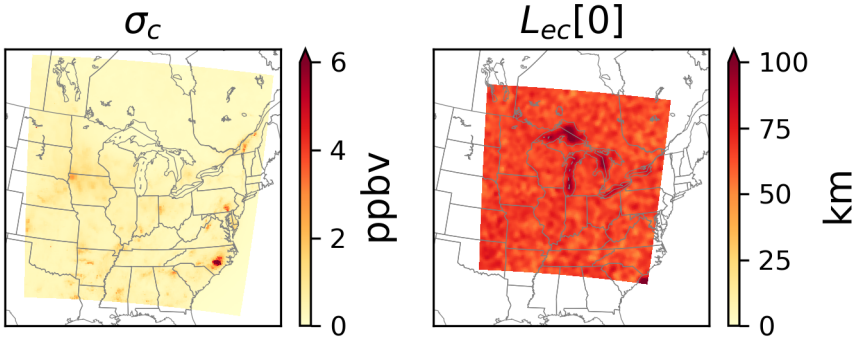


Figure S3. Time means of the surface ammonia concentration error standard deviation σ_c and emissions/surface concentration isotropic correlation length $L_{ec}[0]$ of the GEM-MACH ensemble ammonia error covariance taken over 2015.

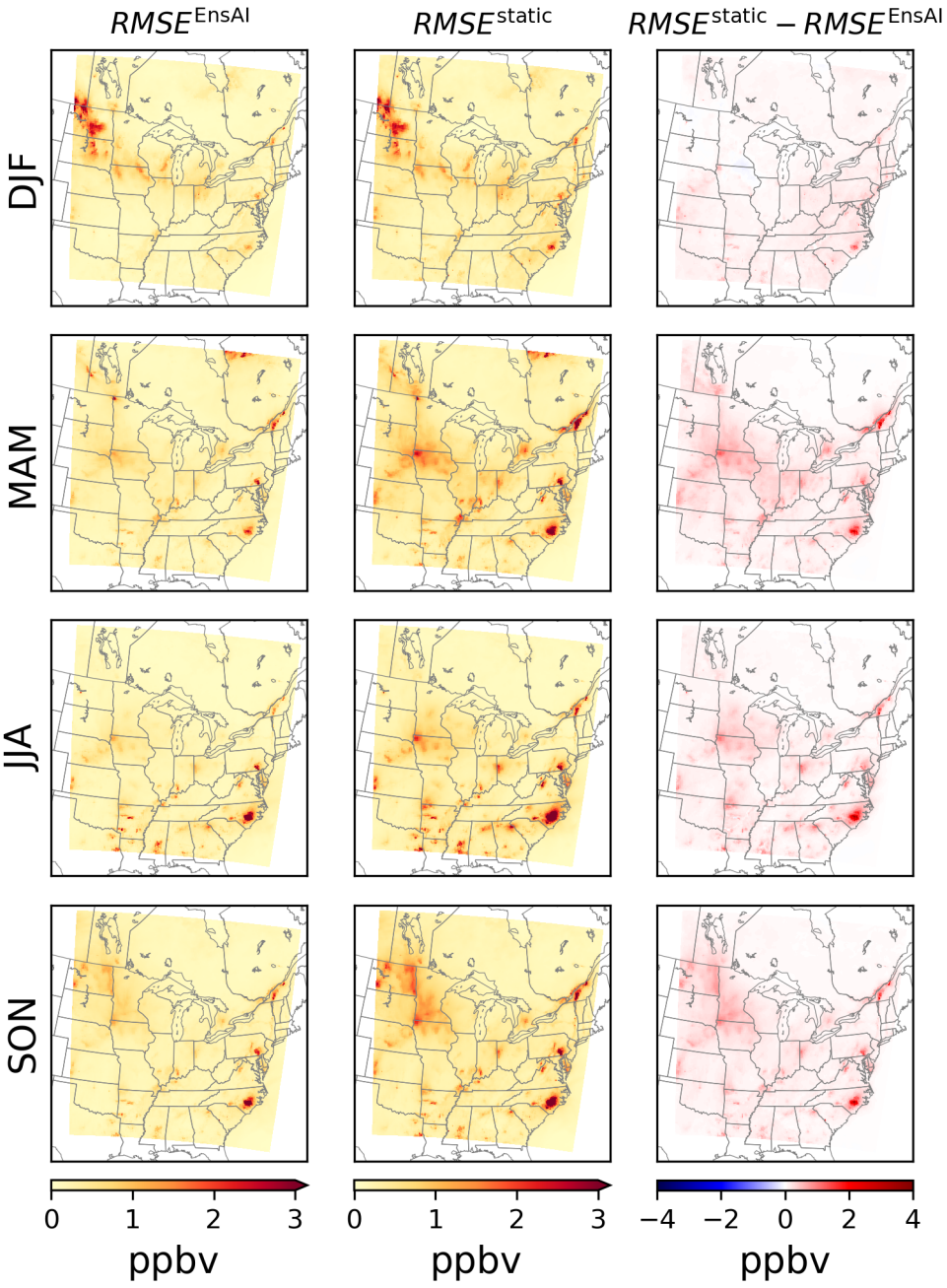


Figure S4. $RMSE$ values for the surface ammonia concentration error standard deviation σ_c for EnsAI (left column), the static error covariances (middle column), and their difference (right column) for December-January-February (DJF), March-April-May (MAM), June-July-August (JJA), and September-October-November (SON) of 2015.

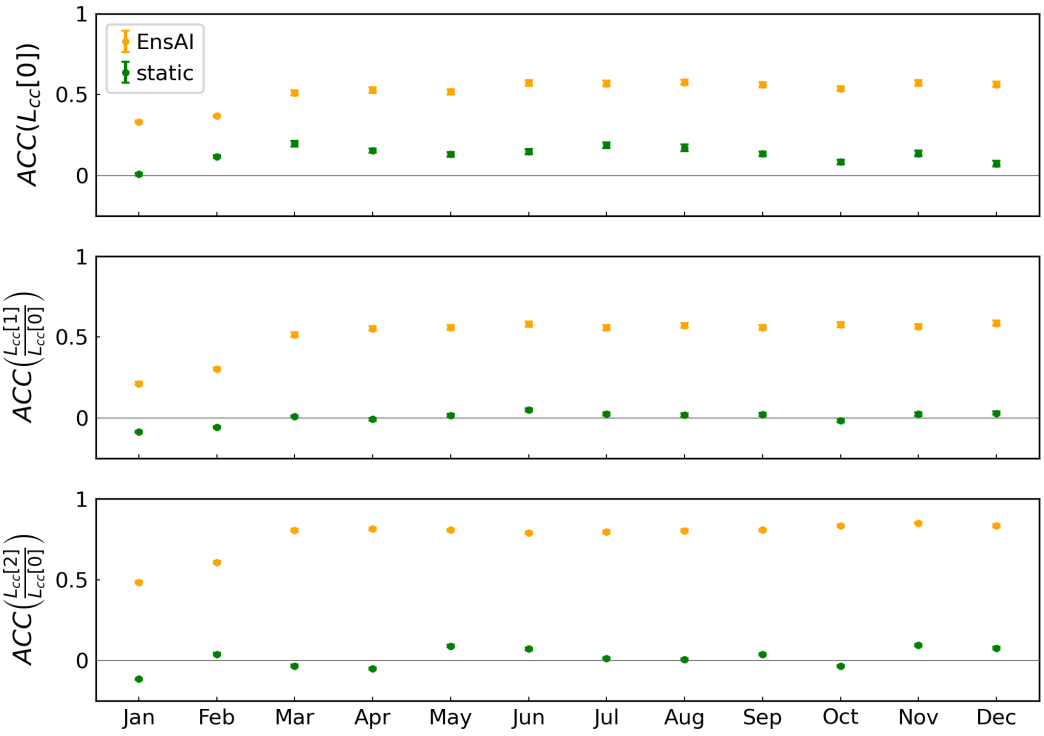


Figure S5. ACC values for $L_{cc}[0]$, $L_{cc}[1]/L_{cc}[0]$, and $L_{cc}[2]/L_{cc}[0]$ over the model domain for each month in 2015.

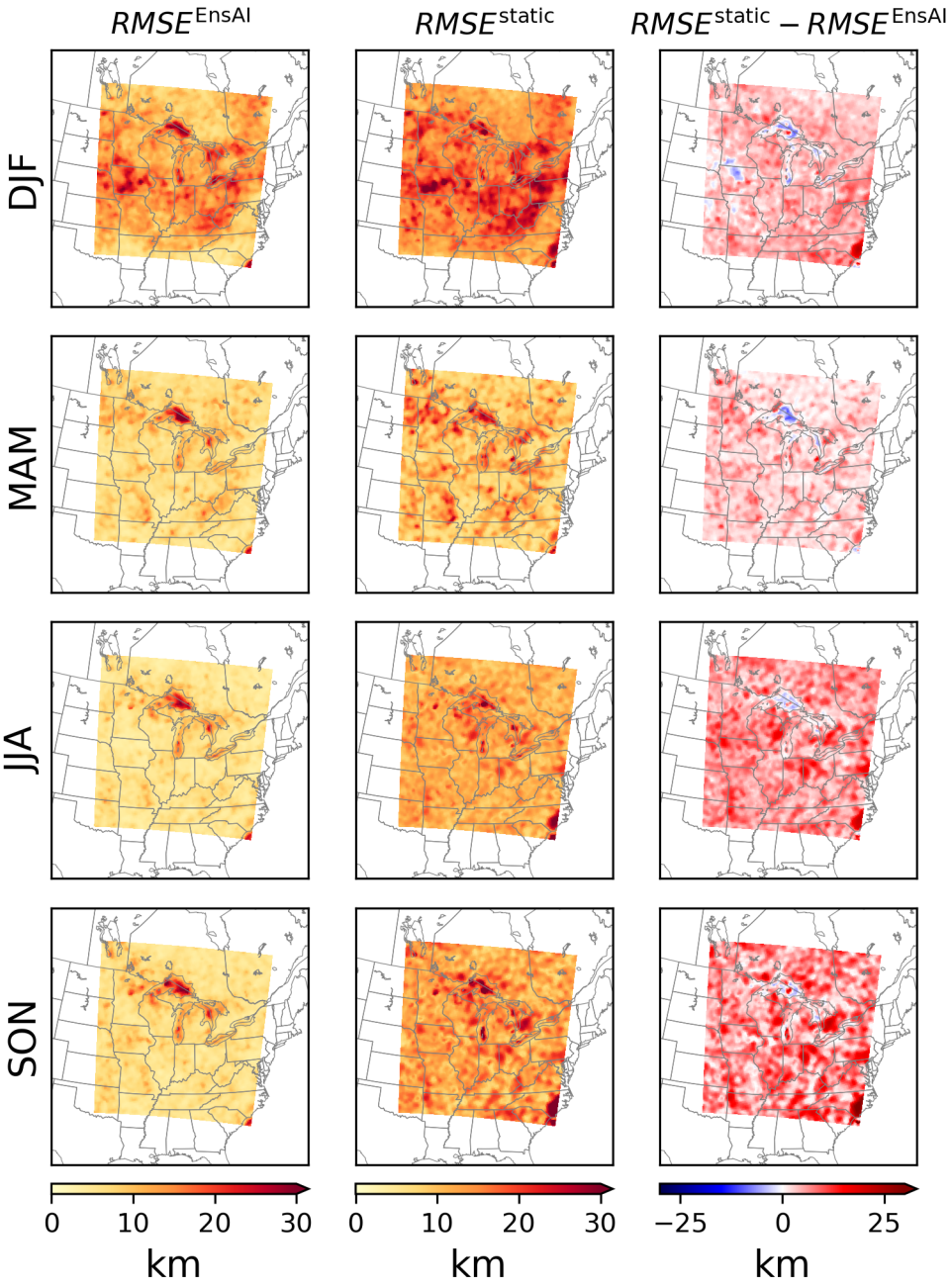


Figure S6. Same as Figure S4 but for $RMSE(L_{ec}[0])$.

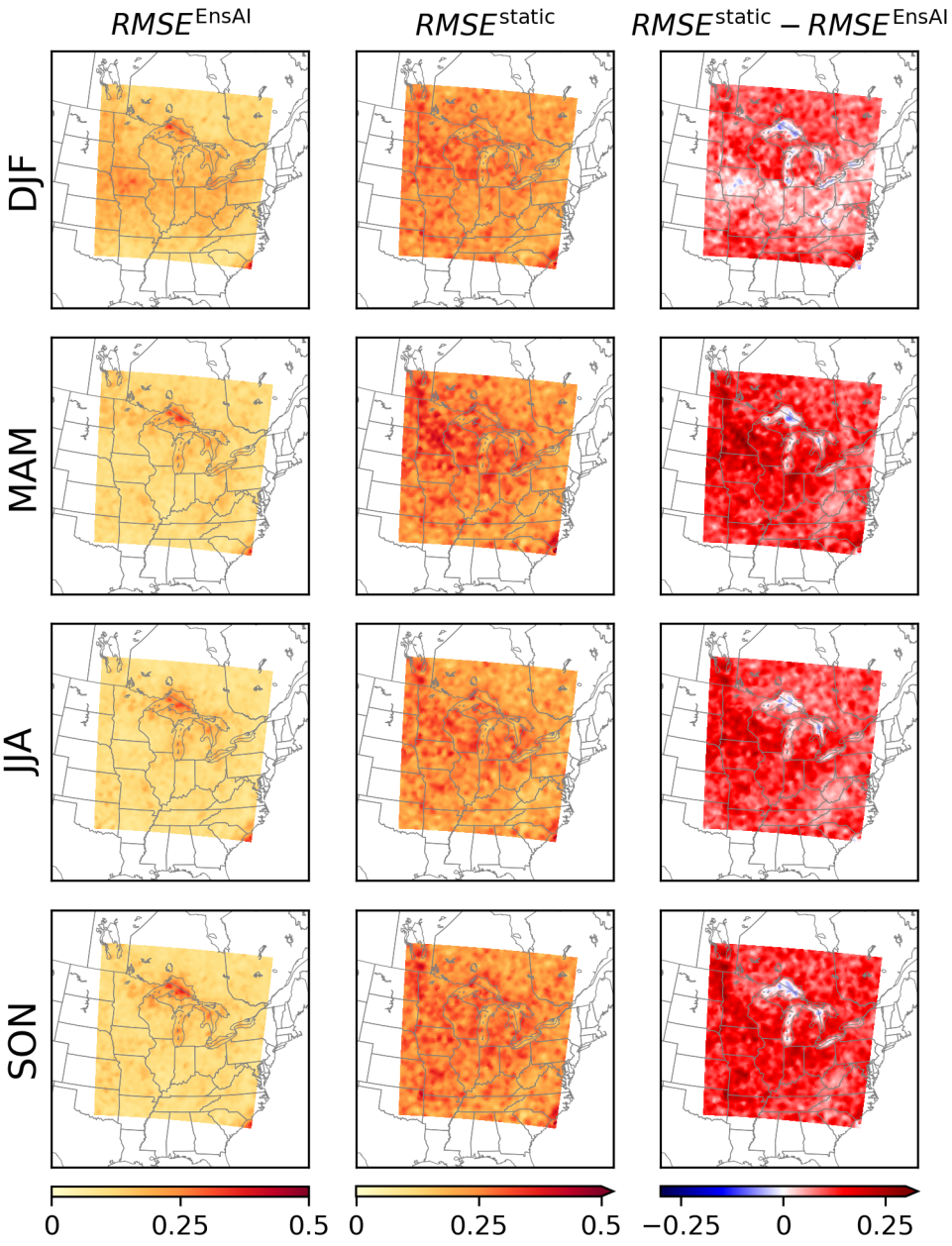


Figure S7. Same as Figure S4 but for $RMSE(L_{ec}[1]/L_{ec}[0])$.

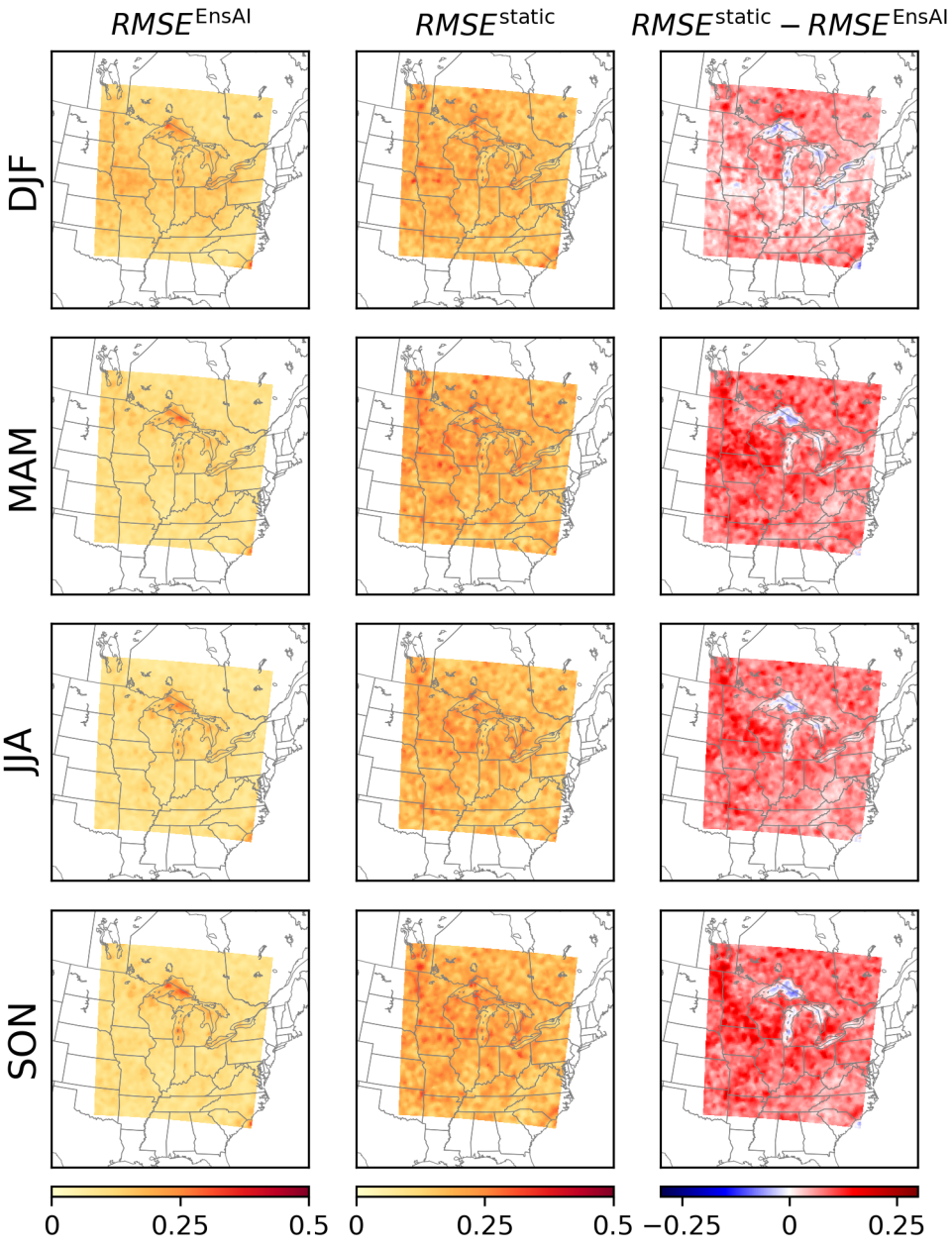


Figure S8. Same as Figure S4 but for $RMSE(L_{ec}[2]/L_{ec}[0])$.

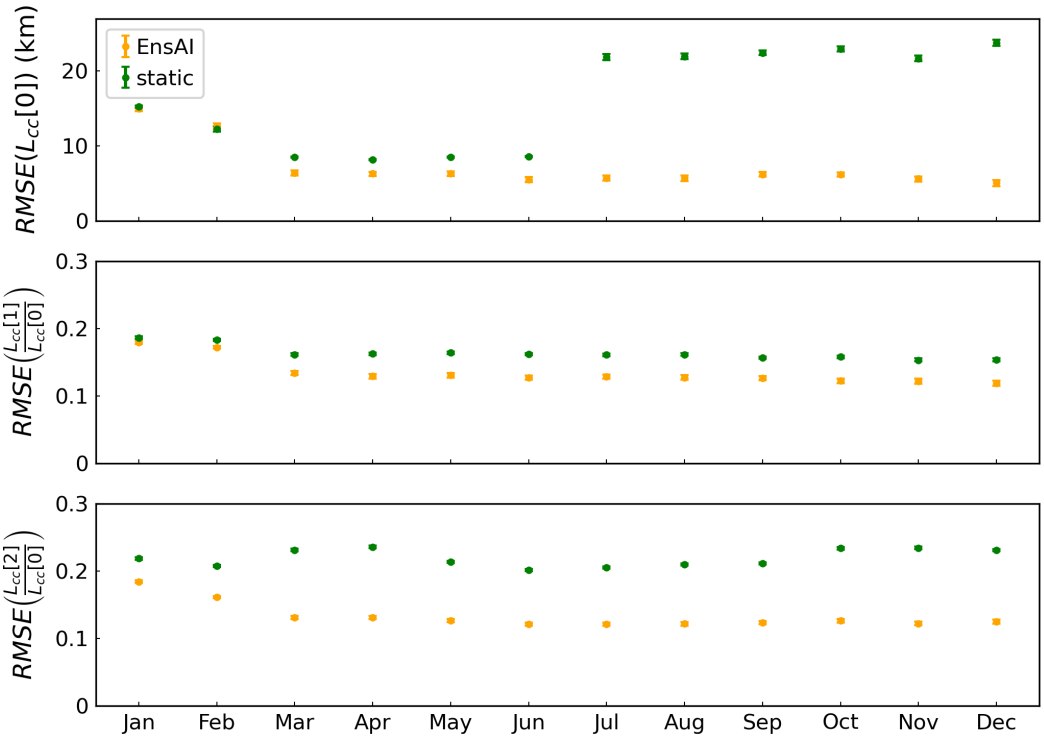


Figure S9. $RMSE$ values for $L_{cc}[0]$, $L_{cc}[1]/L_{cc}[0]$, and $L_{cc}[2]/L_{cc}[0]$ over the model domain for each month in 2015.

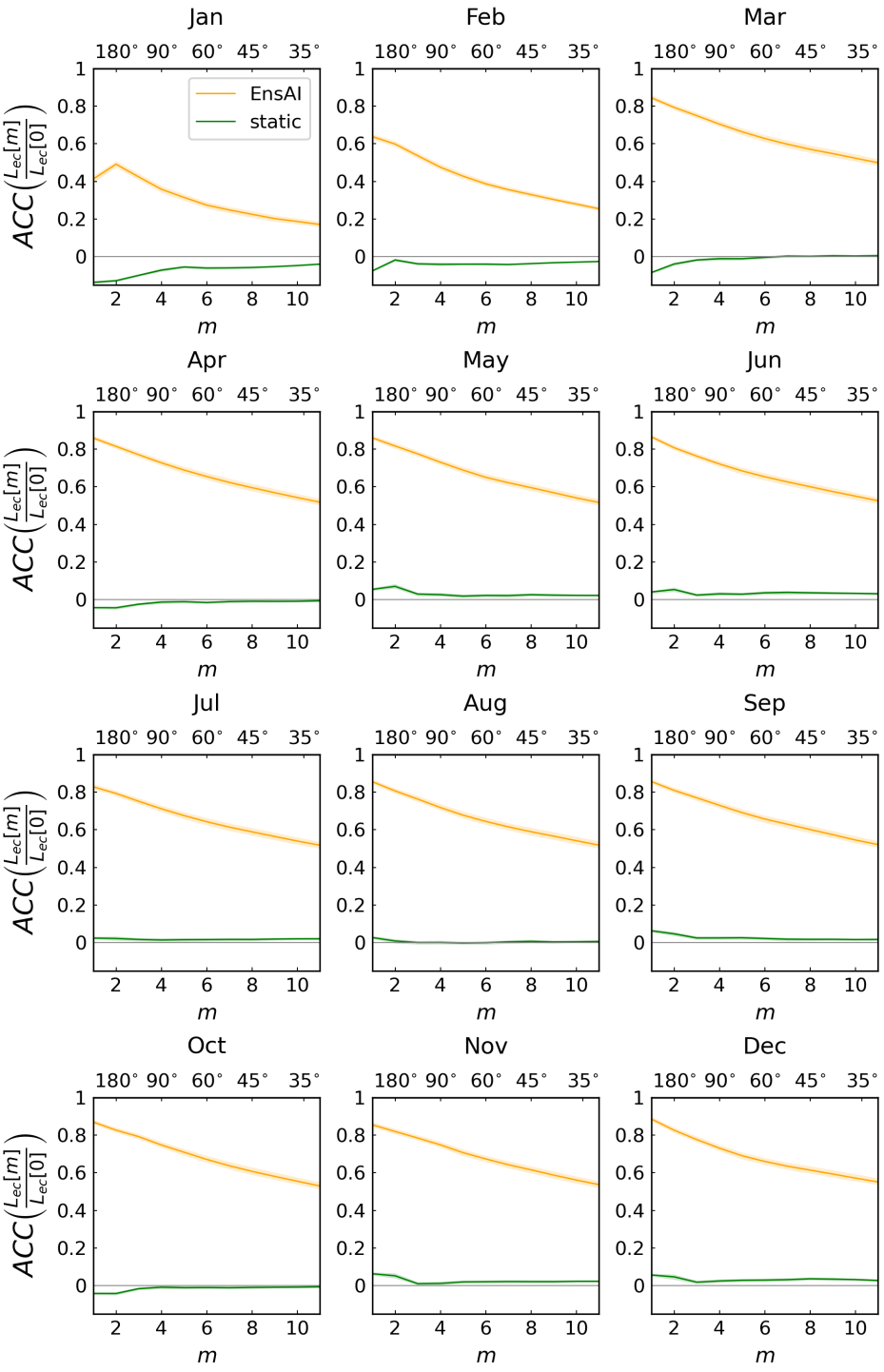


Figure S10. ACC values for the horizontal correlation length modes for the emissions/surface concentration correlation $L_{ec}[m]$ as a function of wavenumber m for EnsAI (orange) and the static covariance (green). The corresponding wavelength of each mode is shown on the upper axis.

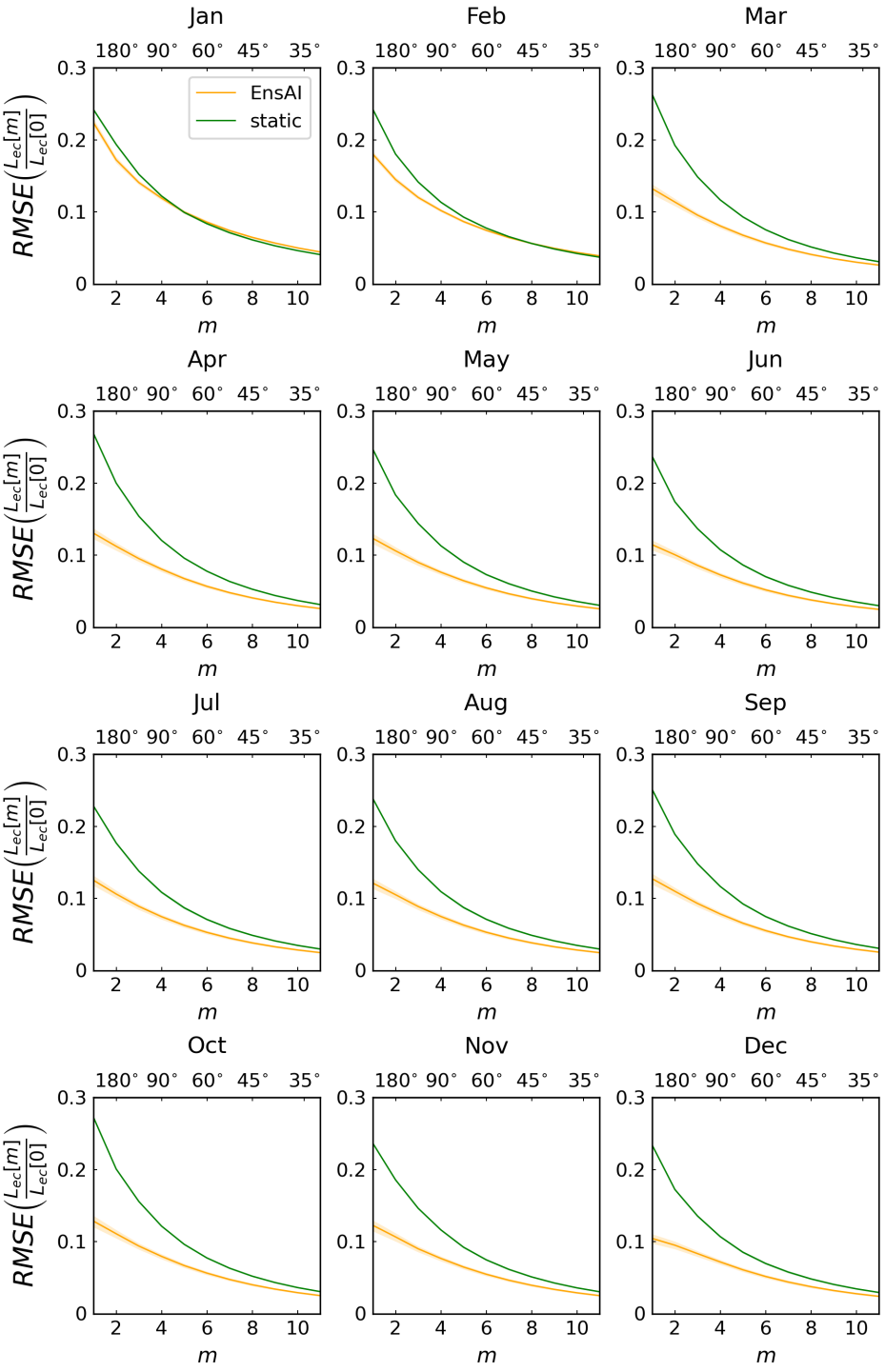


Figure S11. Same as Figure S10 but for the $RMSE$.

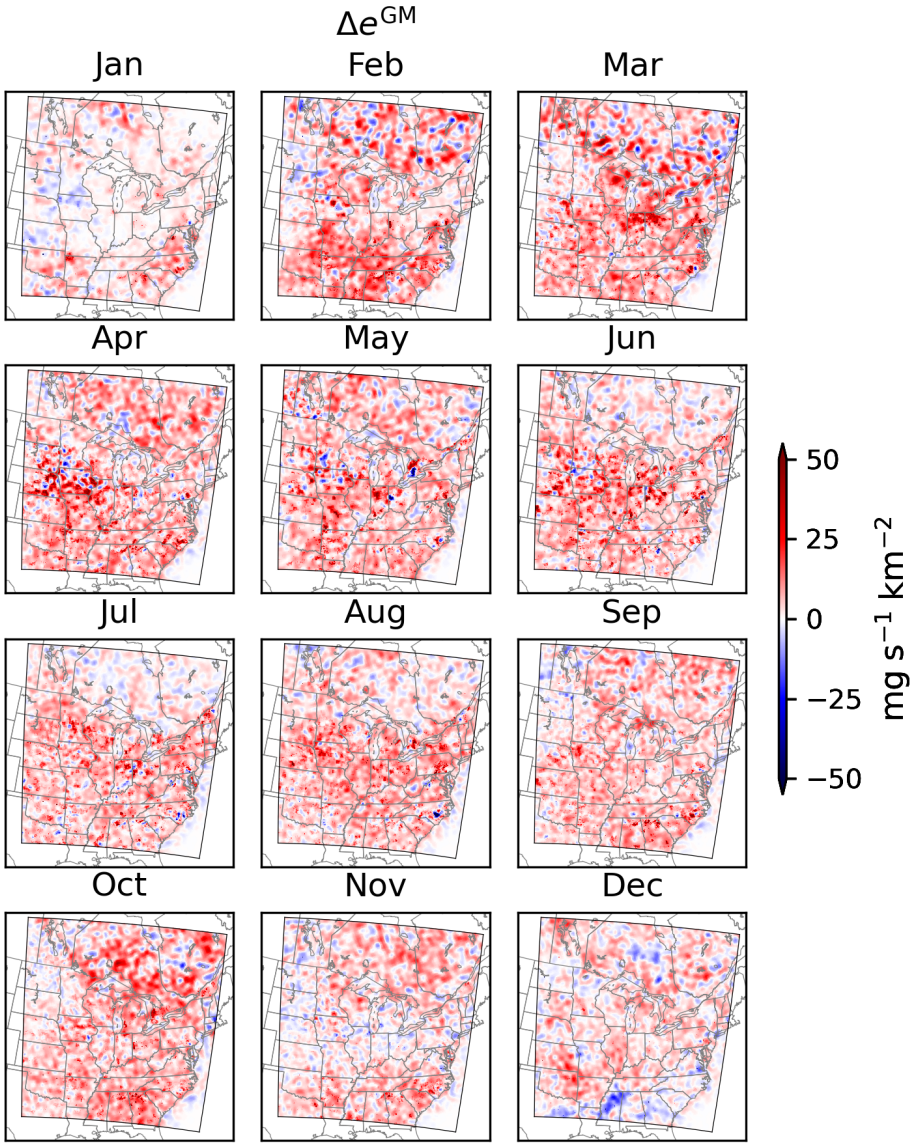


Figure S12. Ammonia emissions increments $\Delta\mathbf{e}^{GM}$ from inversions using the GEM-MACH ensemble to form the background error covariances.

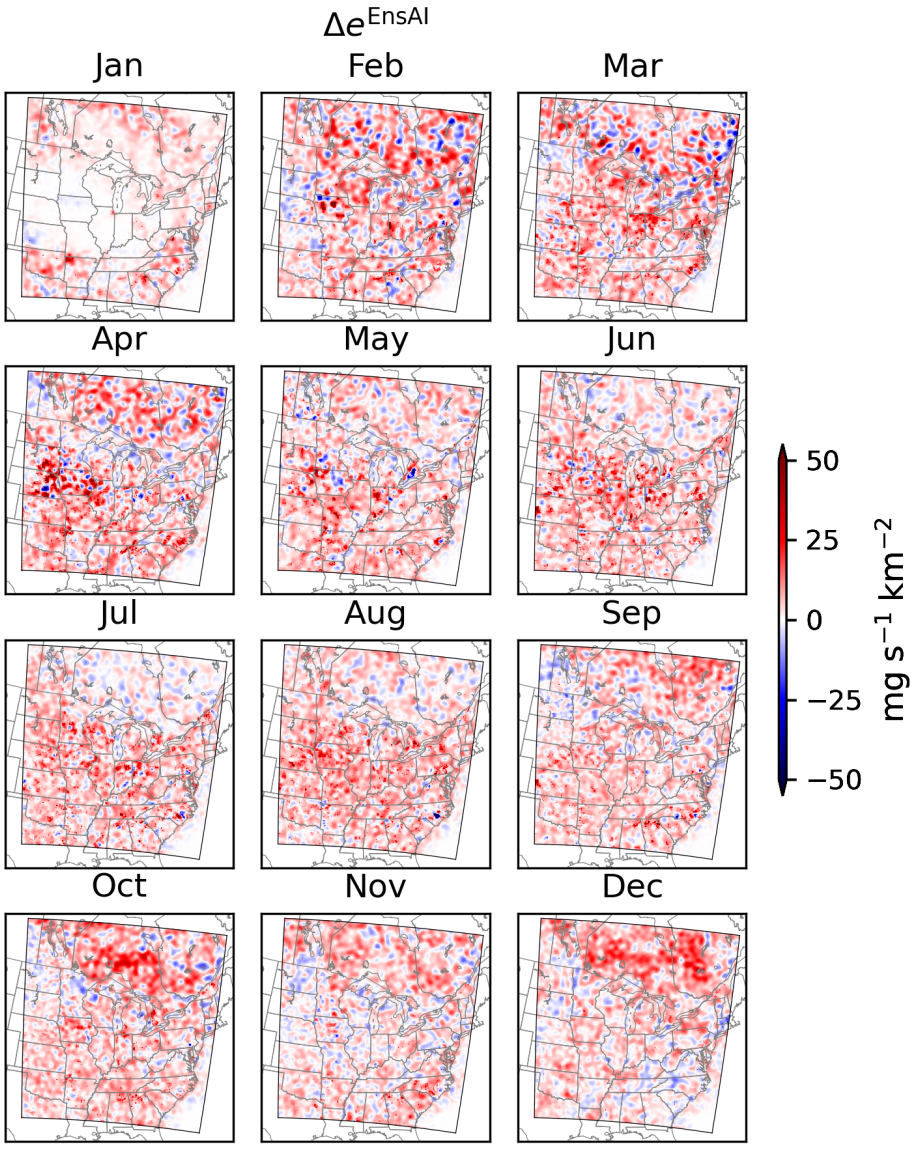


Figure S13. Ammonia emissions increments $\Delta\mathbf{e}^{\mathrm{EnsAI}}$ from inversions using the EnsAI ensemble to form the background error covariances.

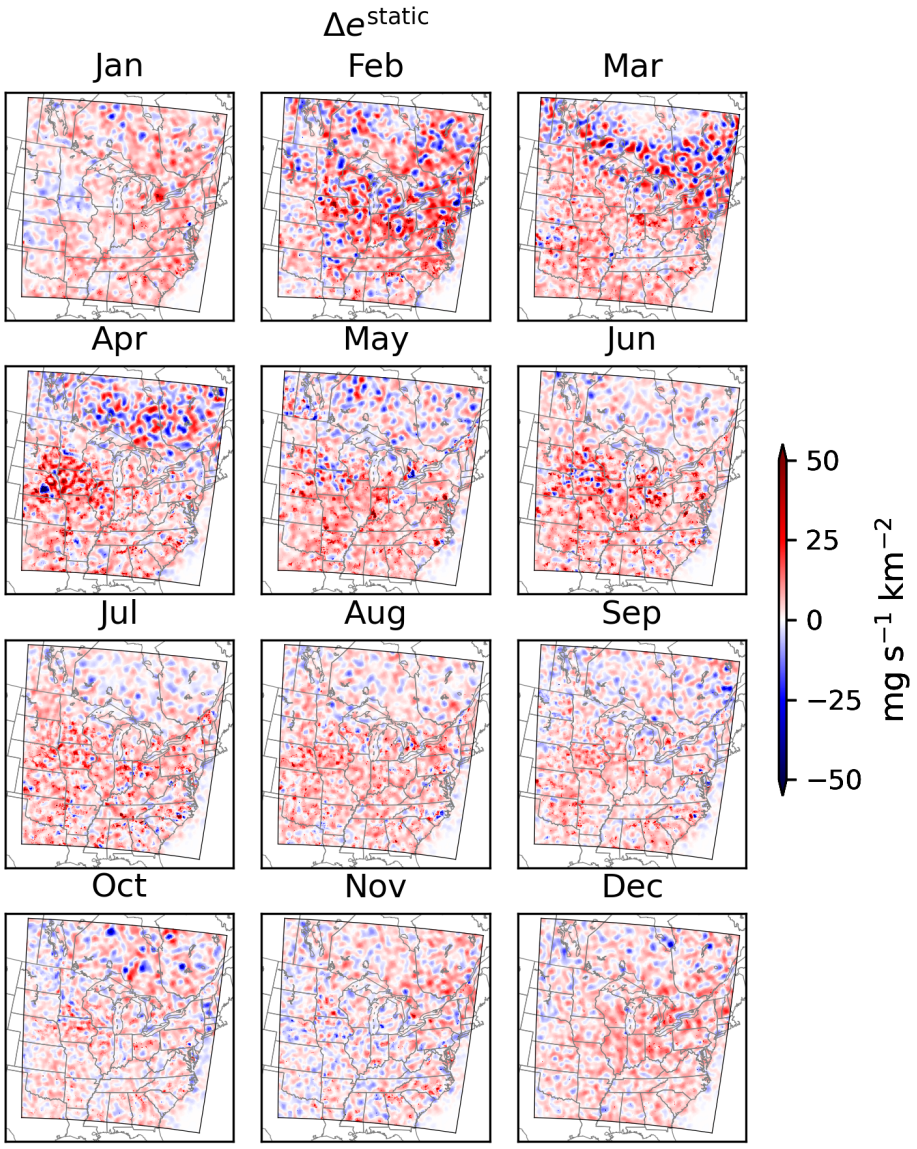


Figure S14. Ammonia emissions increments $\Delta\mathbf{e}^{\text{static}}$ from inversions using the static covariances as the background error covariances.

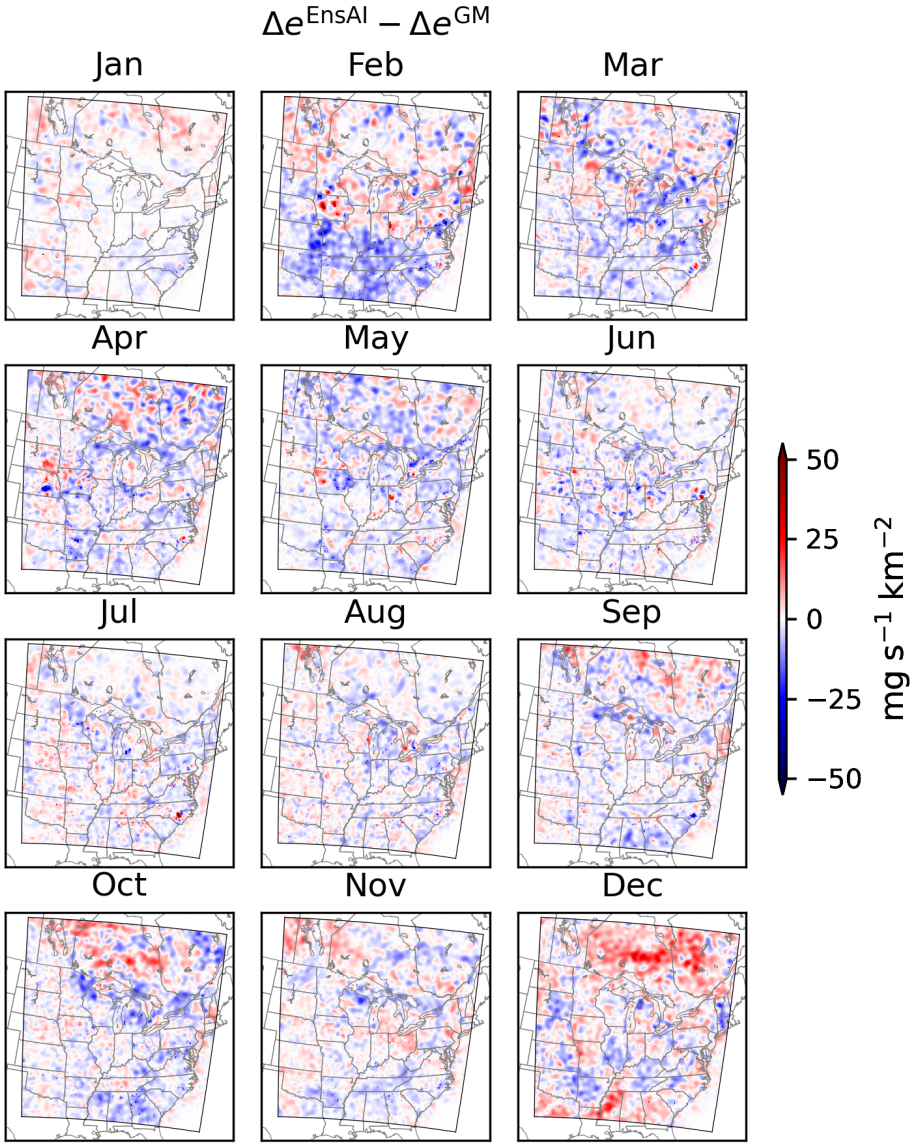


Figure S15. Differences between the ammonia emissions increments from inversions using the EnsAI ensemble ($\Delta\mathbf{e}^{\mathrm{EnsAI}}$) and using the GEM-MACH ensemble ($\Delta\mathbf{e}^{\mathrm{GM}}$).

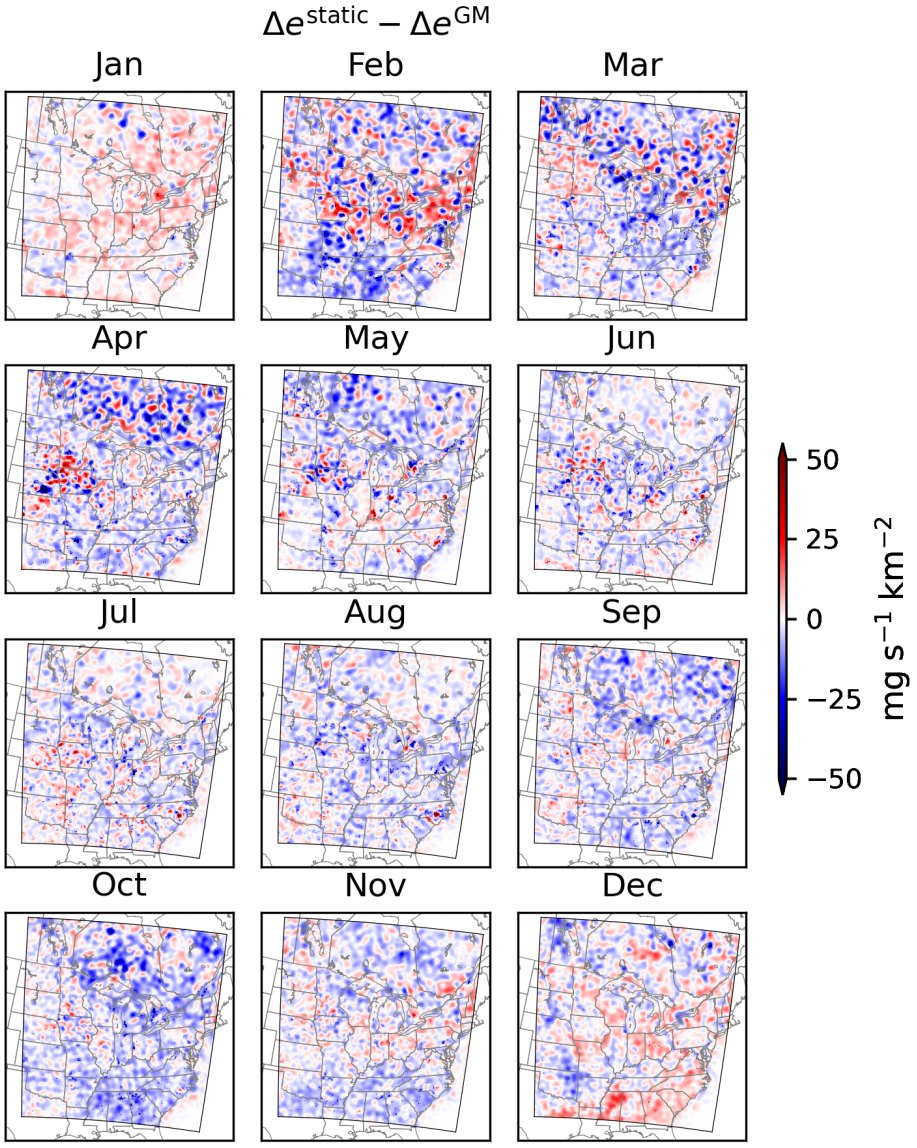


Figure S16. Differences between the ammonia emissions increments from inversions using the static covariances ($\Delta\mathbf{e}^{\text{static}}$) and using the GEM-MACH ensemble ($\Delta\mathbf{e}^{\text{GM}}$).

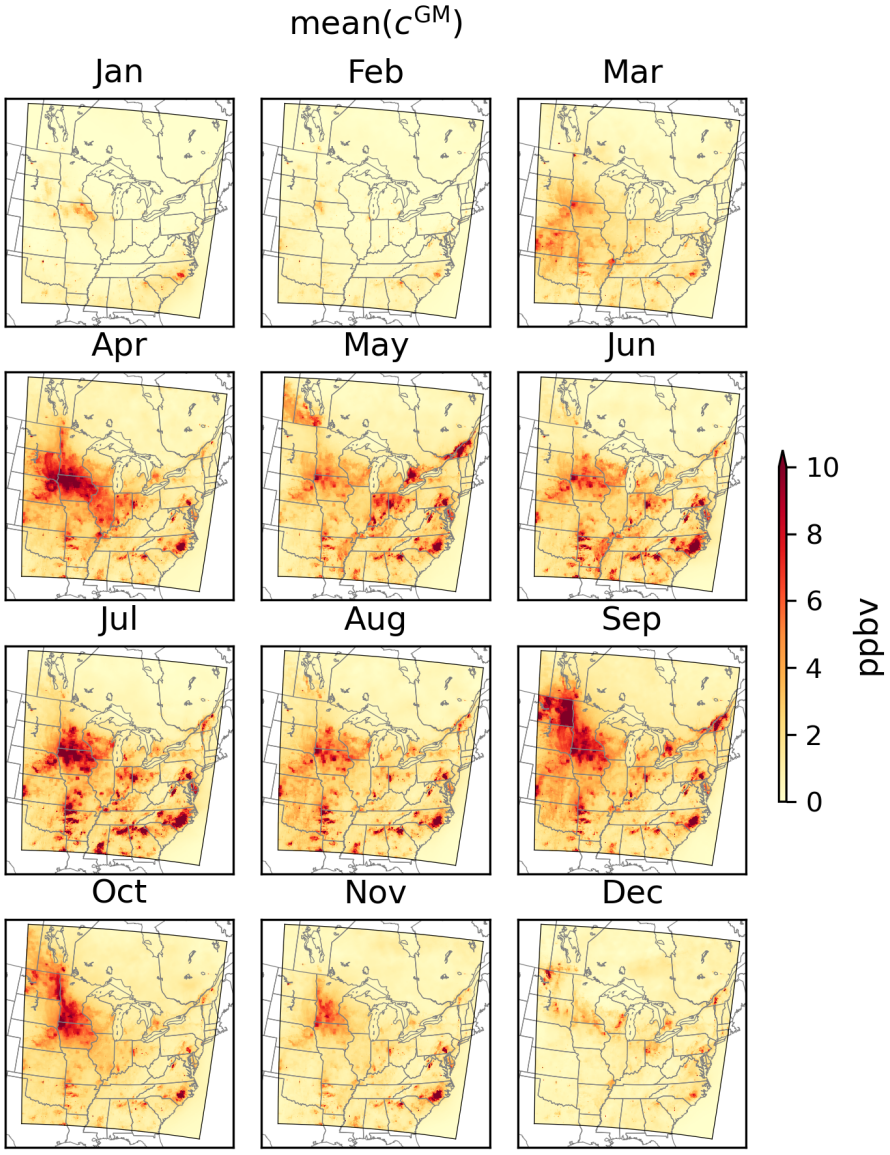


Figure S17. Mean of the posterior ammonia surface concentrations from inversions using the GEM-MACH ensemble.

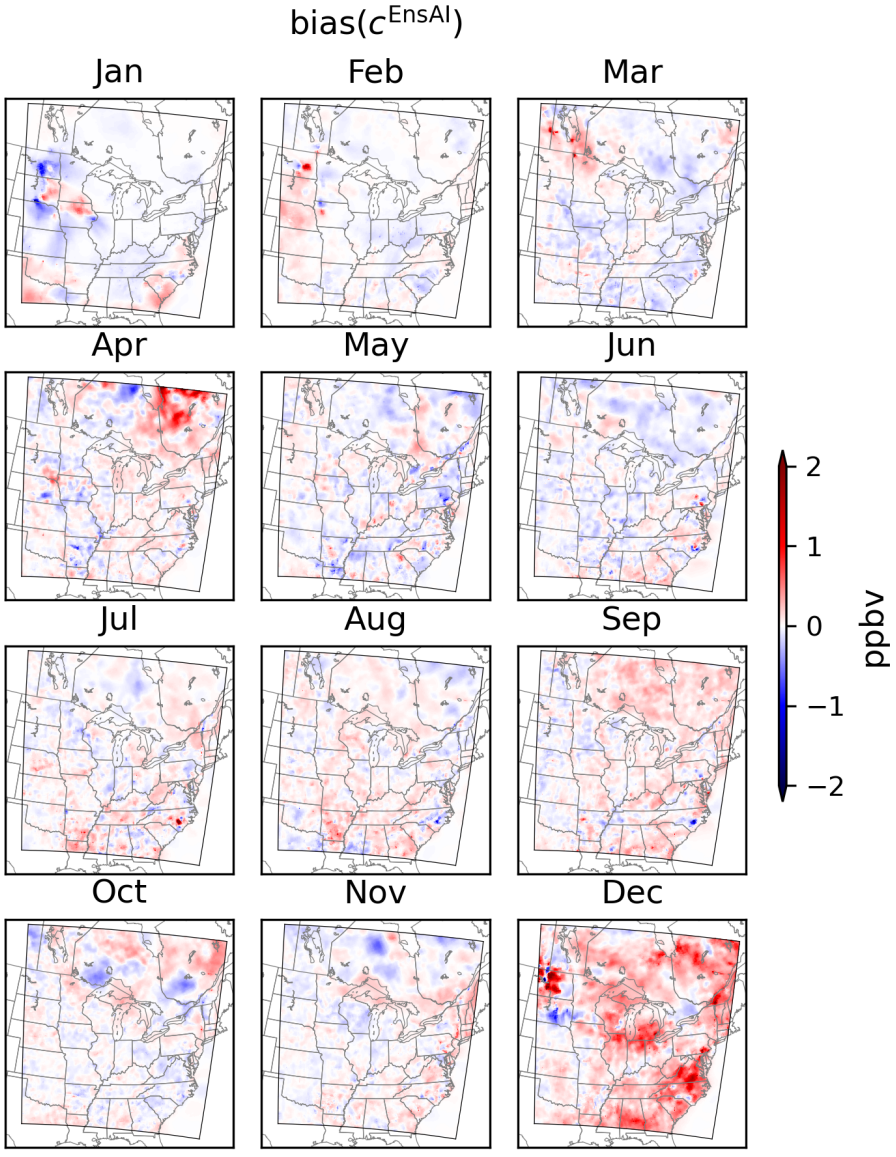


Figure S18. Mean differences between the posterior ammonia surface concentrations from inversions using the EnsAI ensemble and using the GEM-MACH ensemble.

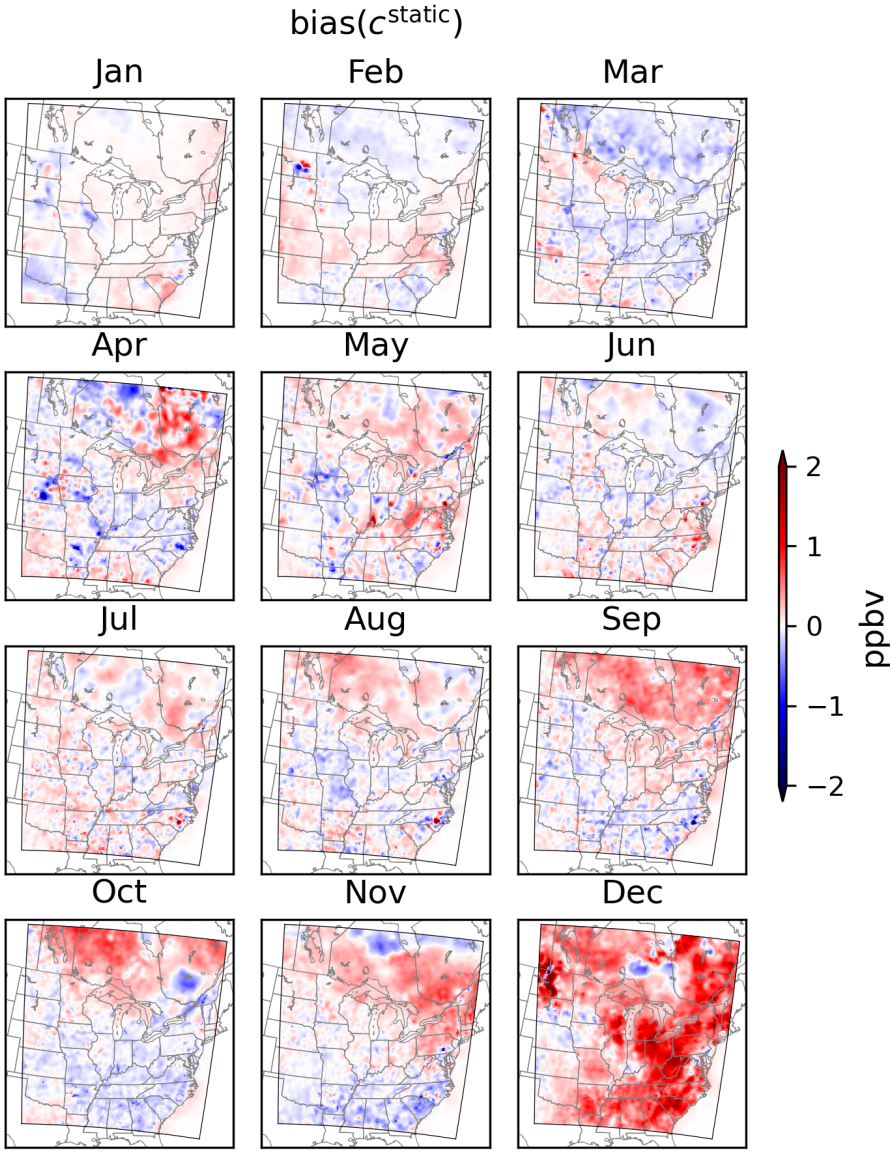


Figure S19. Mean differences between the posterior ammonia surface concentrations from inversions using the static covariances and using the GEM-MACH ensemble.

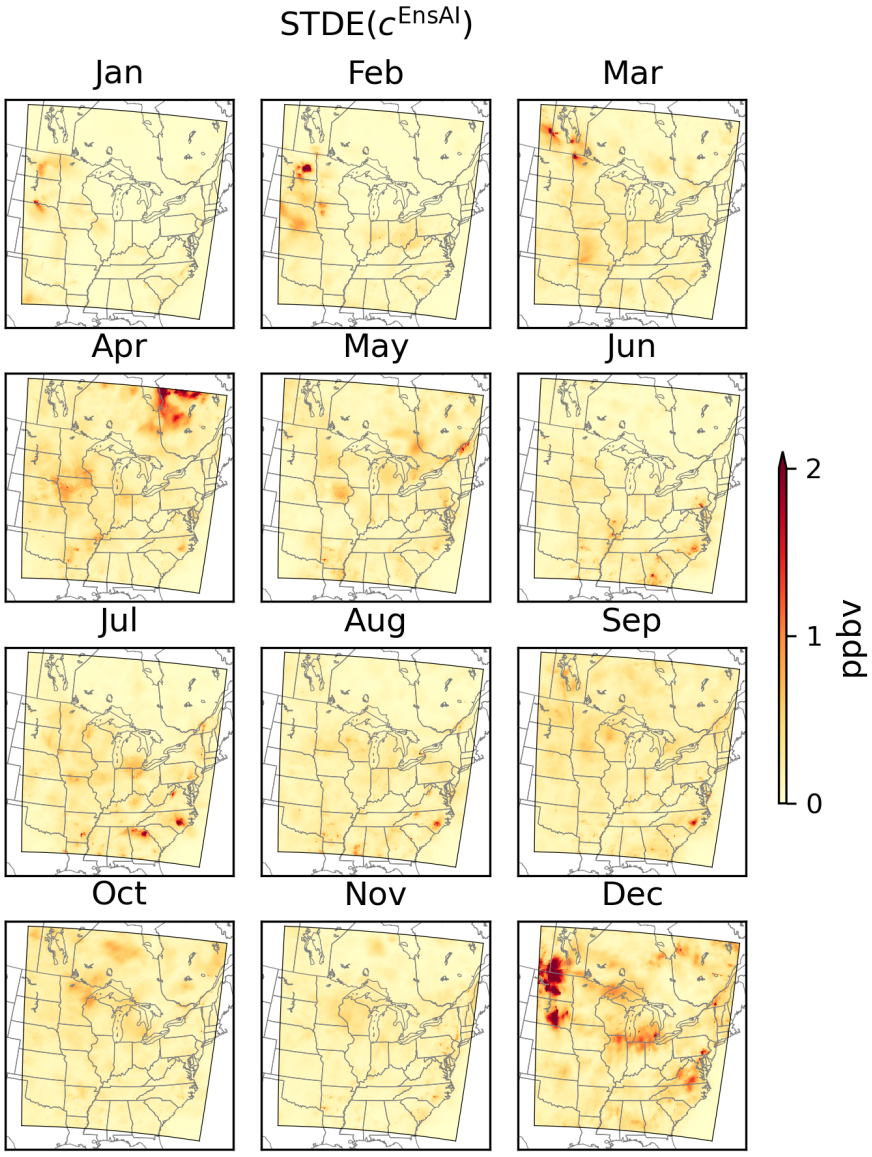


Figure S20. Standard deviation of the differences between the posterior ammonia surface concentrations from inversions using the EnsAI ensemble and using the GEM-MACH ensemble.

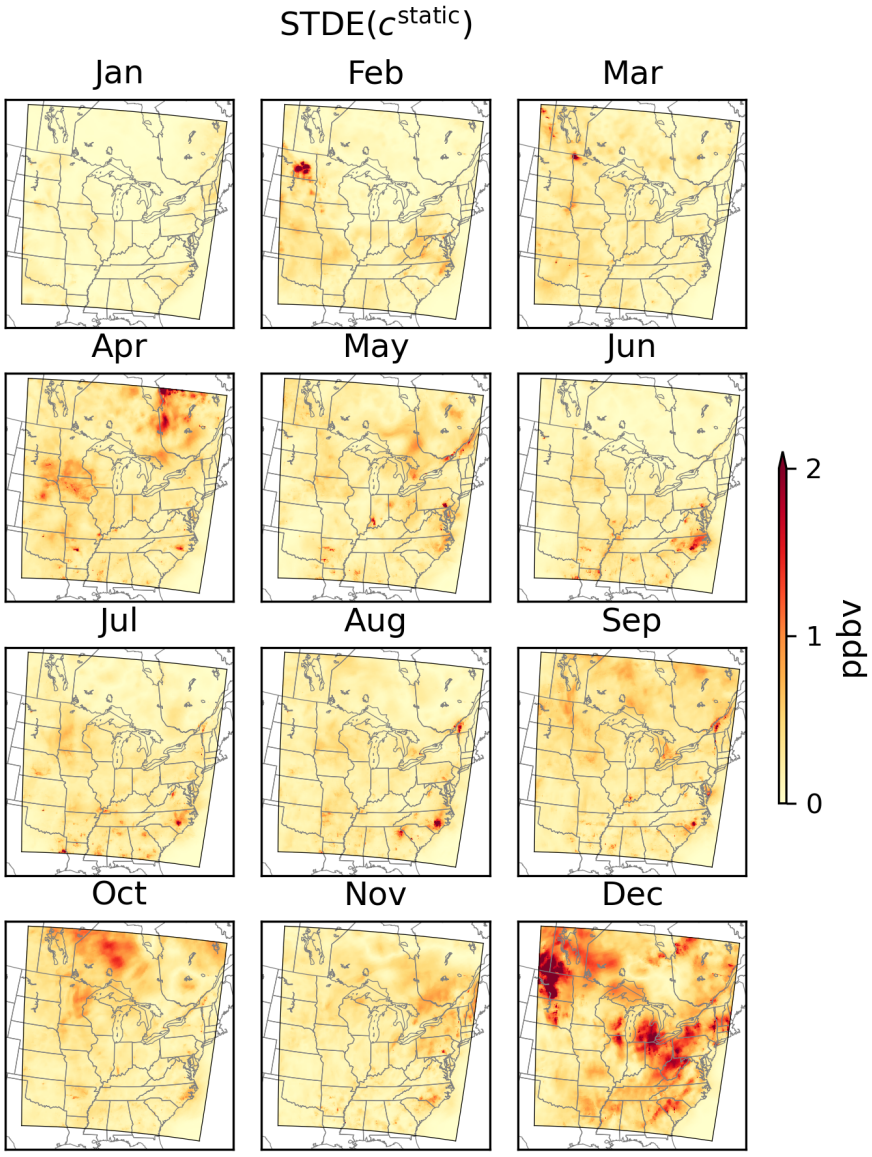


Figure S21. Standard deviation of the differences between the posterior ammonia surface concentrations from inversions using the static covariances and using the GEM-MACH ensemble.

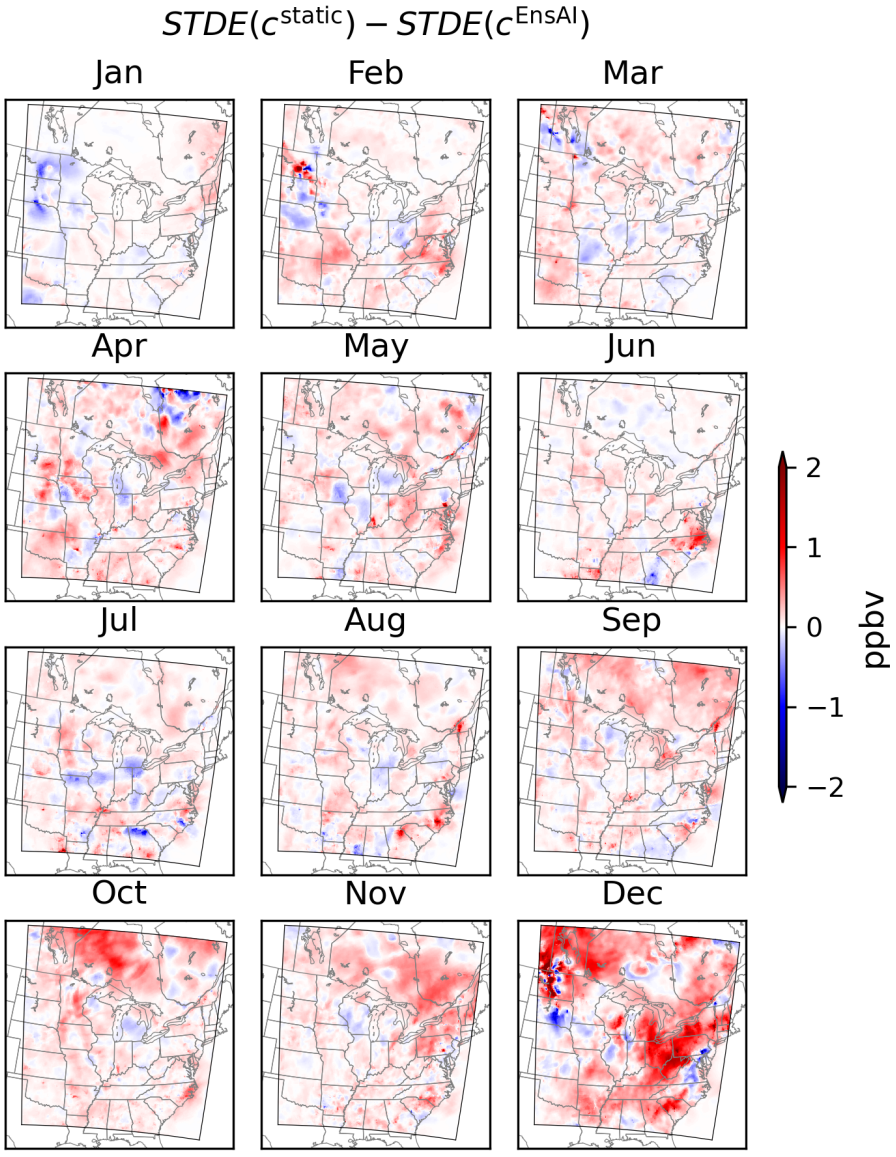


Figure S22. Differences in the $STDE$ of the posterior ammonia surface concentrations between the EnsAI inversions ($STDE(\mathbf{c}^{\text{EnsAI}})$) and the static covariance inversions ($STDE(\mathbf{c}^{\text{static}})$).

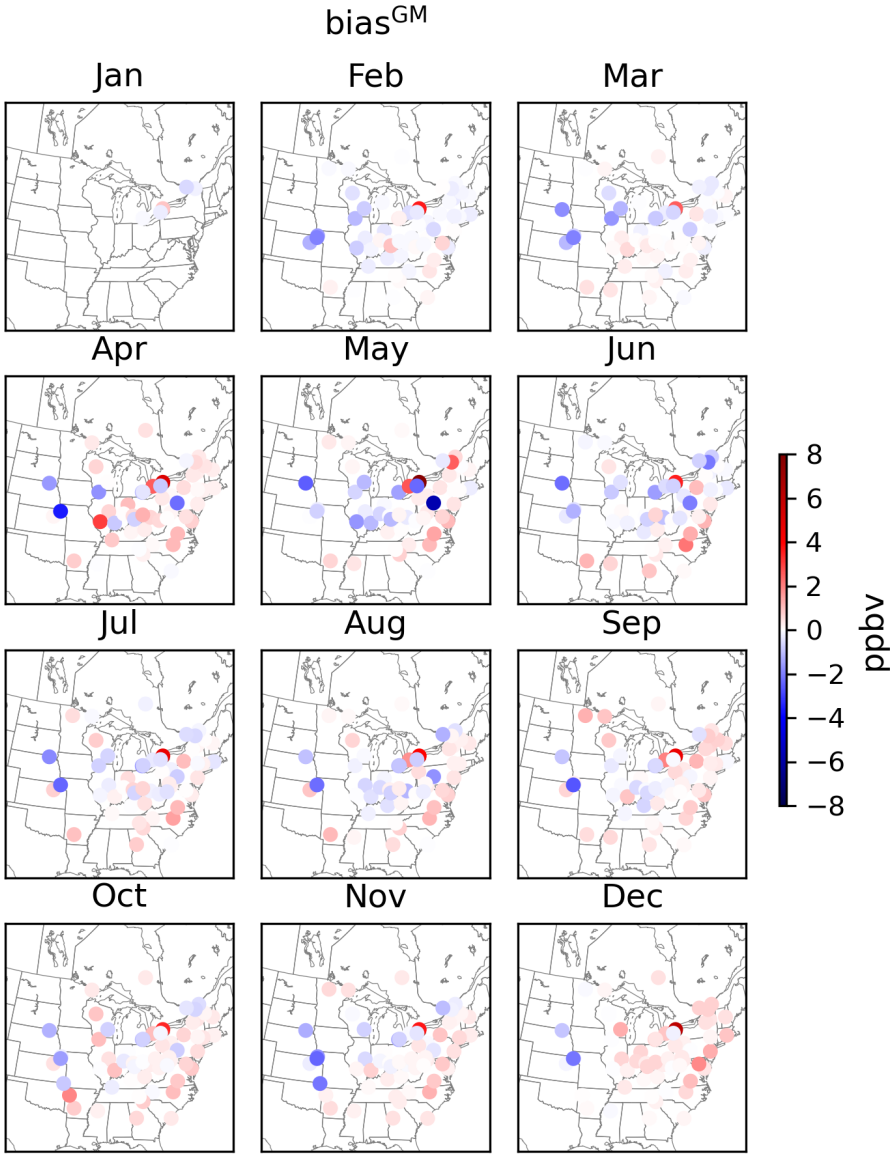


Figure S23. Biases of the posterior ammonia surface concentrations from inversions using the GEM-MACH ensemble (bias^{GM}) in comparison to AMoN and NAPS observations for 2015.

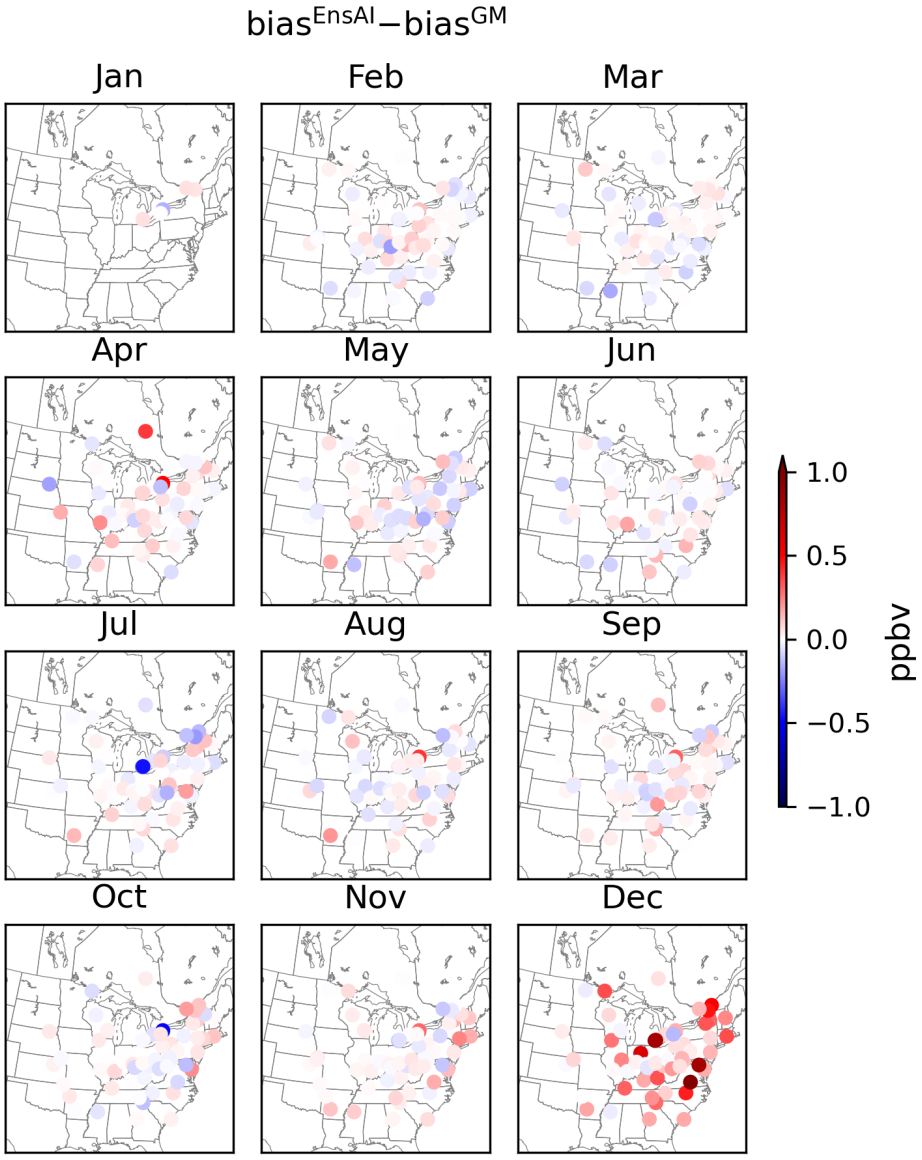


Figure S24. Differences in biases of the posterior ammonia surface concentrations between the EnsAI ($\text{bias}^{\text{EnsAI}}$) and GEM-MACH ensemble (bias^{GM}) inversions for AMoN and NAPS observations for 2015.

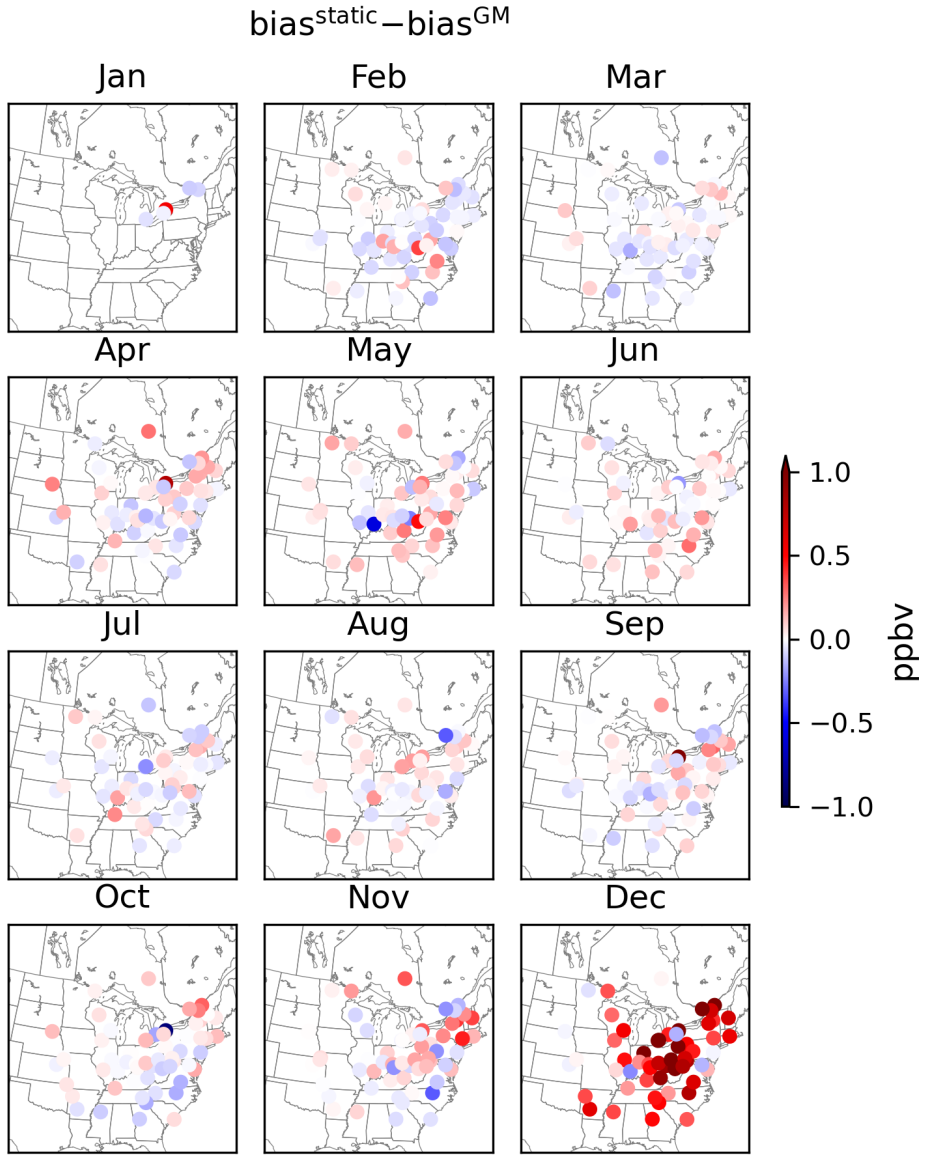


Figure S25. Differences in biases of the posterior ammonia surface concentrations between the static covariances ($\text{bias}^{\text{static}}$) and GEM-MACH ensemble (bias^{GM}) inversions for AMoN and NAPS observations for 2015.

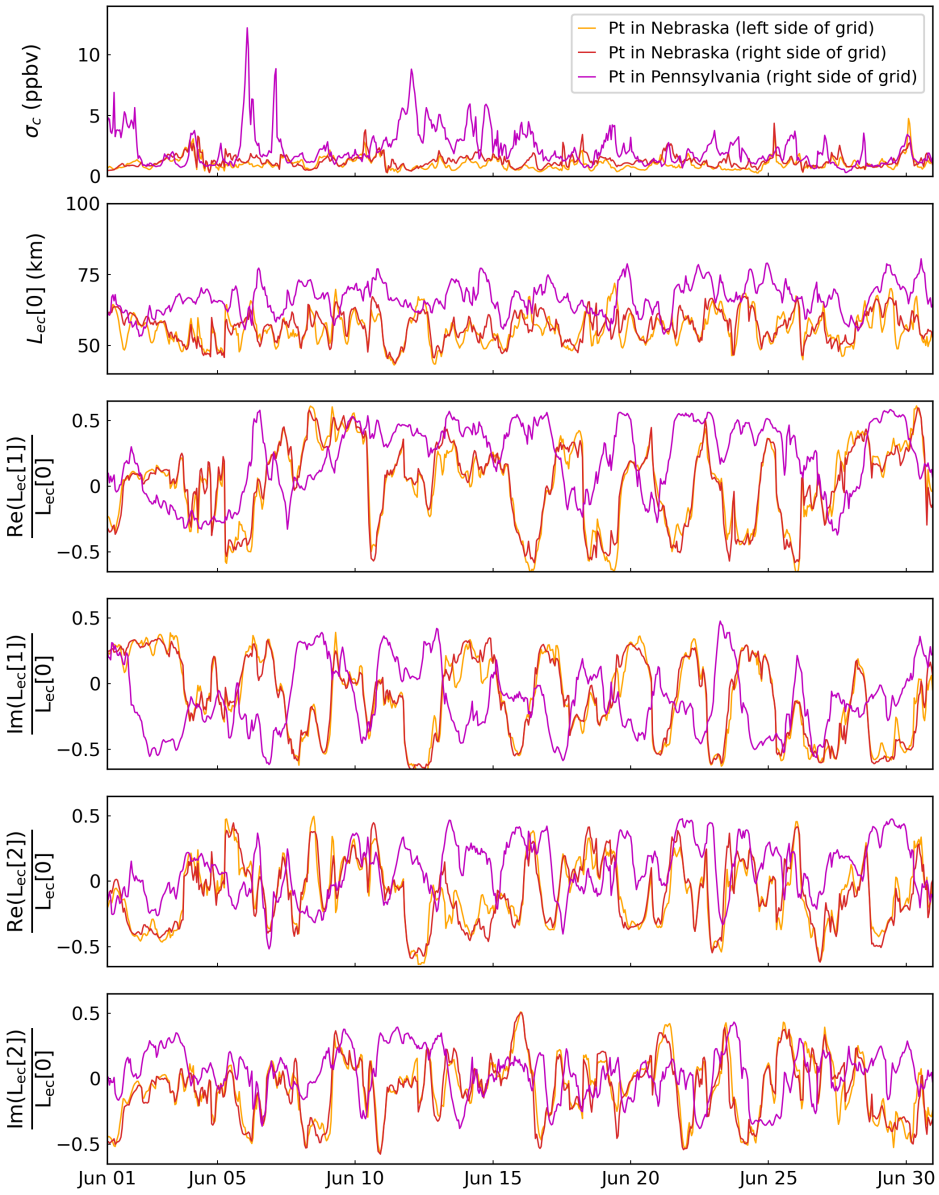


Figure S26. Time series of components of the error covariances for EnsAI in the test of its translational invariance. The orange curves show the error covariance components of the original EnsAI run at a location in Nebraska, which is on the left side of EnsAI's grid. The red curves show the error covariance components for the location in Nebraska when the 90 leftmost values of the input fields are translated to the right side of the grid. In this translation, the location in Nebraska gets translated to a grid point in Pennsylvania. The curves in purple show the covariance components of the location in Pennsylvania in the original EnsAI run.

month	background covariance	bias (%)	$STDE$ (%)	r
Jan	GEM-MACH	-3.9 ± 18.0	43 ± 15	0.46 ± 0.44
	EnsAI	-8.8 ± 15.7	40 ± 13	0.45 ± 0.49
	static	8.6 ± 26.0	59 ± 22	0.44 ± 0.46
Feb	GEM-MACH	8.4 ± 6.9	87 ± 14	0.18 ± 0.06
	EnsAI	7.9 ± 7.1	89 ± 15	0.18 ± 0.06
	static	11.9 ± 7.0	87 ± 14	0.18 ± 0.06
Mar	GEM-MACH	-0.1 ± 4.9	70 ± 10	0.59 ± 0.05
	EnsAI	-0.9 ± 4.8	70 ± 10	0.60 ± 0.05
	static	-2.8 ± 4.8	69 ± 10	0.60 ± 0.06
Apr	GEM-MACH	32.0 ± 14.0	164 ± 22	0.47 ± 0.07
	EnsAI	36.8 ± 14.8	174 ± 25	0.46 ± 0.08
	static	38.4 ± 15.3	180 ± 27	0.44 ± 0.08
May	GEM-MACH	25.6 ± 15.4	182 ± 36	0.59 ± 0.09
	EnsAI	23.7 ± 15.4	182 ± 37	0.59 ± 0.09
	static	29.3 ± 15.4	183 ± 38	0.59 ± 0.09
Jun	GEM-MACH	-5.8 ± 9.1	105 ± 17	0.42 ± 0.07
	EnsAI	-5.3 ± 9.3	106 ± 17	0.40 ± 0.07
	static	-6.3 ± 9.2	106 ± 17	0.39 ± 0.07
Jul	GEM-MACH	21.1 ± 9.8	122 ± 20	0.56 ± 0.05
	EnsAI	24.2 ± 9.7	120 ± 20	0.56 ± 0.05
	static	24.7 ± 9.9	123 ± 21	0.56 ± 0.05
Aug	GEM-MACH	15.1 ± 9.5	116 ± 18	0.53 ± 0.07
	EnsAI	18.5 ± 10.1	122 ± 18	0.52 ± 0.07
	static	17.4 ± 9.9	120 ± 17	0.51 ± 0.07
Sep	GEM-MACH	27.0 ± 6.9	102 ± 15	0.60 ± 0.07
	EnsAI	30.7 ± 7.1	104 ± 16	0.59 ± 0.07
	static	32.9 ± 7.7	112 ± 18	0.58 ± 0.07
Oct	GEM-MACH	23.5 ± 7.9	100 ± 17	0.64 ± 0.06
	EnsAI	19.9 ± 7.3	92 ± 15	0.64 ± 0.06
	static	15.0 ± 6.9	86 ± 13	0.63 ± 0.06
Nov	GEM-MACH	9.9 ± 8.6	109 ± 20	0.47 ± 0.17
	EnsAI	13.2 ± 9.1	115 ± 23	0.47 ± 0.17
	static	16.7 ± 9.1	115 ± 23	0.47 ± 0.17
Dec	GEM-MACH	43.0 ± 11.7	138 ± 46	0.35 ± 0.14
	EnsAI	62.0 ± 12.4	146 ± 44	0.34 ± 0.14
	static	95.8 ± 14.6	170 ± 50	0.33 ± 0.14

Table S1. Comparison statistics between the posterior ammonia surface concentrations and ammonia surface observations from the AMoN and NAPS networks for 2015.